Design, Simulation, and Evaluation of Imaging Oximeters

Steve Dai[1], Ye Tian, Joyce Farrell[2]

Electrical Engineering, Stanford University, Stanford, CA 94305, USA

ABSTRACT

Computer simulations have played an important role in the design and evaluation of imaging sensors with applications in remote sensing [1] and consumer photography [2-7]. In this paper, we provide an example of computer simulations used to guide the design of imaging sensors for a biomedical application: We consider how sensor design, illumination, measurement geometry, and skin type influence the ability to detect blood oxygen saturation from non-invasive measurements of skin reflectance. The methodology we describe in this paper can be used to design, simulate and evaluate the design of other biomedical imaging systems.

Keywords: Oximetry, biomedical imaging, image systems evaluation, imaging sensors

1. INTRODUCTION

As consumer photography matures, more and more engineers are turning their attention to designing biomedical imaging devices. Recently, researchers have invented attachments that transform cell phone cameras into microscopes [8, 9] and optometers [10]. In addition, there are numerous studies demonstrating that non-invasive hyperspectral imaging of diffuse skin reflectance can be used to date bruises[11], diagnose skin diseases [12], monitor wound healing [13] and, in general, characterize tissue perfusion [14-17]. These two types of imaging systems, the inexpensive and ubiquitous RGB imaging sensor and the more expensive hyperspectral and multispectral imagers, bound the range of commercially available spectrophotometric devices that are available today.

Recent advances in sensor technology [18, 19] give engineers many new sensor design options. Simulation enables the engineer to design and evaluate systems that take advantage of these new technologies even before they become more economically viable. To illustrate the power of system simulation in the design and optimization of new imaging devices, we use the Image Systems Evaluation Toolbox (ISET) [2, 3] to explore and evaluate the design of an imaging oximeter.

2. OXIMETRY

2.1 Conventional oximeters

Oximeters are pervasive in hospital settings where they are used in a wide variety of applications ranging from monitoring the amount of blood oxygenation during artificial respiration in surgery to weaning patients from ventilators. They are used to monitor the health of a mother and her fetus during childbirth and to determine neonatal care after birth. They are used to assess the viability of tissue transplants and the progress in wound healing. Oximeters are also used in a variety of non-medical applications such as monitoring pilots at high altitudes and athletes during exercise.

The design of oximeters takes advantage of the fact that oxygenated and deoxygenated blood absorbs light in different wavelengths[20]. Since oxy-hemoglobin and deoxy-hemoglobin have different spectrophotometric signatures [21, 22], it is possible to quantify the ratio of oxygenated to deoxygenated blood (referred to as blood oxygen saturation or S_{O2}) by the ratio of the amount of light absorbed at the different wavelengths.

---

[1] stevedai@stanford.edu
[2] joyce_farrell@stanford.edu

Pulse oximeters compare the amount of light absorbed at two wavelengths during the peak of the arterial pulse. The reflected and transmitted light in one waveband, referred to as the isosbestic wavelength, does not change when hemoglobin molecules bind with oxygen. The reflected and transmitted light in the other non-isosbestic waveband does change when hemoglobin is oxygenated or deoxygenated. Oximeters calculate the ratio of light absorbed by the non-isosbestic wavelength to that of the isosbestic wavelength. This ratio is invariant over a small range of skin types and measurement geometries.

Most pulse oximeters are transmissive devices that shine light in narrow bands (typically generated by light emitting diodes, LEDs) from one side of a finger and measure the amount of light that is received (and not absorbed) by a sensor (typically a photodiode) placed at the other side of the finger. Reflective pulse oximeters can project light on any region of the patient's body and measure the amount of light that is reflected back and thus not absorbed in the body.

The oximeter signal-to-noise ratio (SNR) is determined by the power spectra of the LEDs, particularly the peak and width of the spectral power. It is important to use narrowband lights that discriminate between the oxy-hemoglobin and deoxy-hemoglobin spectral signatures. However the more narrow the bandwidth, the lower the SNR of the imaging device. SNR is further reduced when other materials in skin tissue layers, such as melanin, water, fat and lipids, absorb or scatter light.

2.2 Imaging oximeters

Pulse oximeters use photodiodes rather than CMOS or CCD spatial arrays. While all of these sensors are based on silicon, photodiodes have higher quantum efficiency in the near-infrared (NIR) regions. The two spectral channels in a pulse oximeter are created with LED lights. The design of oximeters has thus been limited by the spectral power of commercially available LED lights. Typically, oximeters use an LED with peak sensitivity at 940 nm and a half-amplitude bandwidth of 50 nm as the isosbestic channel and an LED with peak sensitivity at 660 nm and a half-amplitude bandwidth of 20 nm as the non-isosbestic channel.

More recently, there has been growing interest in designing imaging oximeters that provide a spatial image of the distribution of oxygenated hemoglobin. Researchers have used RGB [23], multispectral [24] , and hyperspectral imaging systems [13, 14, 25] to visualize the hemodynamics of subsurface skin tissues. Engineers have many options for designing imaging oximeters. They can use a monochrome sensor array with sequentially flashing LED lights [26] or they can use a single broadband illuminant with multiple spectral filters [27]. They can use spectrally tunable imaging sensors [15, 16] and/or a combination of different illuminants and imaging sensors. Whether spectral imagers are created by varying illumination or the spectral transmissivity of color filters, one wonders how many spectral channels are necessary. The answer to this question will depend on the spectral power of the illumination, the spectral transmissivity of filters between the illuminated object and the sensor, and the spectral sensitivity of the sensor array.

In this paper we use image systems simulation technology to evaluate the design choices and tradeoffs by quantifying the performance of two-channel imaging oximeters. We vary the peak wavelength sensitivity and waveband of two spectral channels and analyze their performance in predicting blood oxygenation levels.

3.   IMAGE SYSTEMS SIMULATION

The ISET [2, 3] simulations include representations of the scenes, optics, sensors, and image processing.

3.1 Scene

The reflectance spectroscopy of human skin in the visible range of wavelengths is primarily determined by the light absorbed by chromophores in the epidermis (melanin) and dermis (hemoglobin) and by the light scattered by cells and collagen fibers in these two layers of skin. In fact, light reflected in wavelengths ranging between 480 nm and 700 nm can be predicted by

$$R(\lambda) = 10^{-[(w_1 \times HbO(\lambda)) + (w_2 \times Hb(\lambda)) + (w_3 \times M(\lambda)) + K]} \tag{1}$$

where $HbO(\lambda)$, $Hb(\lambda)$, and $M(\lambda)$ are spectral functions (Figure 1) describing the absorbance coefficients for oxy-hemoglobin, deoxy-hemoglobin, and melanin, respectively; w_1, w_2, and w_3 are weights representing the relative saturations of these chromophores; and K is a factor representing the effects of light scatter [13]. We validate this characterization of skin by fitting experimentally measured skin reflectances from 70 individuals to the model $R(\lambda)$ to

obtain the weights w_1, w_2, and w_3 estimated for each measured reflectance. The estimated reflectances generated by these weights are then compared to the experimentally measured reflectances. From Figure 2, we see that the estimated reflectances are highly correlated ($r = 0.9982$) with the 70 skin reflectances that were measured between 480 and 700 nm.

Oxygen saturation (S_{O2}) is estimated by the ratio of the amount of oxy-hemoglobin to the total amount of hemoglobin ($w_1/(w_1 + w_2)$). We expect this ratio to be constant for all healthy individuals; however the estimates for S_{O2} ranged between 0.4 and 0.8. The variance in the estimates can be explained by the observation that the weights for oxy-hemoglobin (w_1) and melanin (w_3) are negatively correlated ($r = -0.8311$). Individuals with darker skin have higher values for w_3, as would be expected. The negative correlation between w_1 and w_3 is also expected. Melanin resides in the superficial layers of skin. Thus, when more light is absorbed by melanin, less light reaches the deeper layers of the skin where it can be absorbed by hemoglobin. This is the reason why oximeters are less accurate for individuals with dark skin[28, 29].

When we only consider individuals with $w_3 < 0.6$, the mean oxygen saturation across individuals is 0.5301. This value is lower than one would measure using a conventional pulse oximeter. However, pulse oximeters calculate blood oxygen saturation at the peak signal strength of the arterial pulse. The skin reflectance measurements were averaged over time and represent the oxygen in subcutaneous arteries and veins. Our estimates are within the range of other reported studies that estimate blood oxygen saturation from time-averaged hyperspectral images of skin [11].

The predictions of the linear skin model are consistent with our measurements of skin reflectances within the 480 nm to 700 nm window of interest (see Figure 2), but the correlation between estimated and measured reflectance decreases as we introduce wavelengths longer than 700 nm where water and lipid absorb relatively more light. For our purposes, the failure of the linear skin absorbance model at these longer wavelengths does not influence the results of our simulations because the spectral sensitivity of CMOS imagers decreases rapidly beyond 700 nm. Nonetheless, we restrict our analysis to skin reflectances within the range of 480 nm to 700 nm.
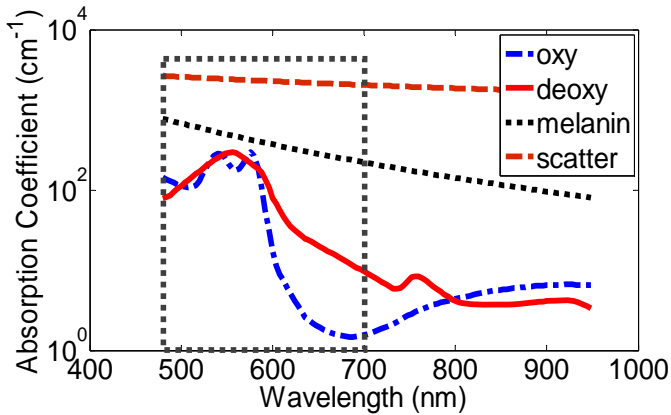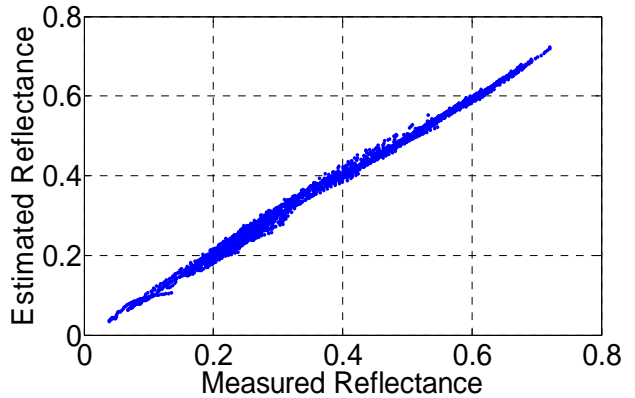

Figure 1: Spectral absorbance function

Figure 2: Measured versus modeled reflectance

With (1) as the skin model, we vary the amount of oxy-hemoglobin (w_1), deoxy-hemoglobin (w_2), melanin (w_3) and scatter (K) to simulate different skin reflectances for our experiment. Because oximeters rely on the assumption that blood volume is constant, we set $w_2 = 1 - w_1$. Since blood oxygen saturation, S_{O2}, is quantified by $w_1/(w_1 + w_2)$ and $w_1 + w_2 = 1$, we can use w_1 to quantify the level of S_{O2}. Figure 3 and 4 show skin reflectances that have different levels of S_{O2}, melanin, and scatter. Notice that for any combination of S_{O2}, melanin, and scatter levels, the reflectances at different oxy/deoxy ratios remain equal at several isosbestic wavelengths. Thus, there are several candidate wavelengths (500 nm, 528 nm, 548 nm, and 570 nm) for the isosbestic sensor channel. Similarly, wavelengths showing variation in reflectance (560 nm and 580 nm) serve as good candidates for the non-isosbestic sensor channel.
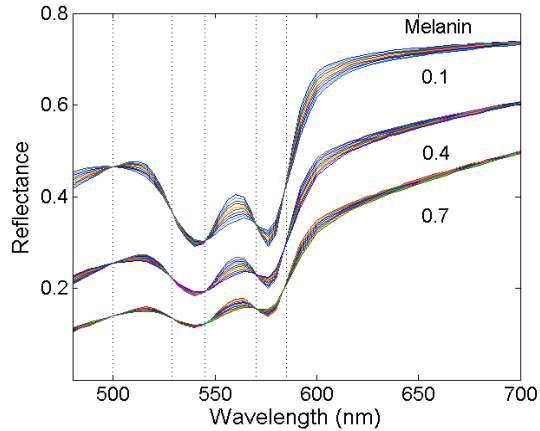
Figure 3: Varying S_{O2} at three melanin levels and constant scatter. Isosbestic wavelengths are demarcated with dashed vertical lines.
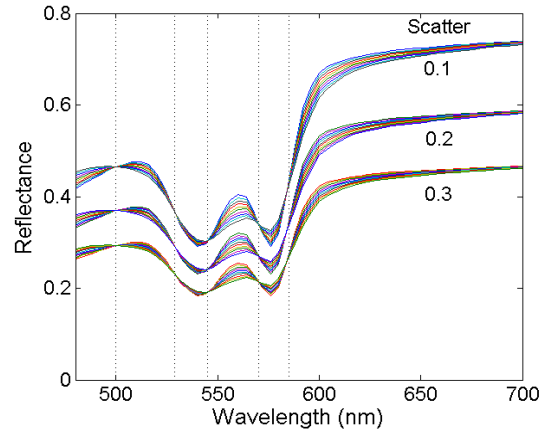
Figure 4: Varying S_{O2} at three scatter levels and constant melanin. Isosbestic wavelengths are demarcated with dashed vertical lines.

3.2 Optics

We create an optical image of the scene subtended on the sensor using diffraction limited optics with f/# of 4.0 and focal length of 3.86 mm.

3.3 Sensors

A pulse oximeter uses a single photodiode rather than CMOS or CCD spatial arrays. The two spectral channels in a pulse oximeter are created with LED lights. The design of pulse oximeters has thus been limited by the quantum efficiency of the photodiode and the spectral power of commercially available LED lights.

We model an imaging oximeter that has peak sensitivities at the isosbestic and non-isosbestic wavelength, respectively. Sensor channels are modeled as Gaussian functions of wavelength that differ in peak sensitivity and bandwidth. In the simulations we report here, the bandwidths of the spectral channels vary between 5 nm and 15 nm, with pixel size of 2.8 microns and sensor noise limited to photon noise. (We will consider the effect of pixel size and different sources of sensor noise in future simulations.) We keep the peak wavelength sensitivity of one channel fixed (referred to as the reference channel) while varying the peak wavelength of the second channel (referred to as the test channel). We used ISET simulations to predict the output (volts) of the reference and test channels for skin reflectance stimuli with different S_{O2} levels. We calculate the correlation between the ratios of responses of the two spectral channels and the S_{O2} levels.

Unlike pulse oximeters that have a single pixel photodiode, we use a CMOS imaging array[3]. We refer to our sensor as an imaging oximeter because it has the potential to measure the spatial distribution of blood oxygenation. In this paper, we evaluate the effects of the peak sensitivity and bandwidth of a two-channel imaging oximeter and discuss the implications of our results for sensor design.

3.4 Processing

We estimate oxygen saturation by the ratio of the responses of isosbestic and non-isosbestic channels. In a separate paper, we will compare this approach with more general linear methods for estimating oxygen saturation from the response of two or more spectral channels.

4. ANALYSIS AND RESULTS

Computer simulations make it possible to explore a very large design space for imaging systems. We constrained our search of the design space in the following way: We simulated the performance of a two-channel imaging oximeter by

---

[3] We used the spectral sensitivity functions for the Micron MT9M001 CMOS Digital Image Sensor reported in http://download.micron.com/pdf/datasheets/imaging/mt9m001_1300_mono.pdf

keeping the peak sensitivity of one channel constant (centered on an isosbestic wavelength and referred to hereafter as the reference channel) while varying the peak sensitivity of the second channel (hereafter referred to as the test channel). In our initial simulations, we set the melanin and scatter coefficients to be low (0.2 and 0.1, respectively) in order to focus on the spectral properties of the reference and test channels. Figure 5 shows the squared correlation coefficient (r^2) between the ratio of sensor responses and S_{O2} expressed as the percentage of the variance explained, $r^2 * 100$) plotted as a function of the peak sensitivity of the test channel. In this example, the reference channel had peak sensitivity at 500 nm (an isosbestic wavelength). Obviously, when the test wavelength is equal to the reference wavelength, it is not possible to predict the S_{O2} levels.

Figure 5 summarizes the results of a simulation in which we found that the best peak sensitivity for the reference and test channels is 500 and 560 nm, respectively. This result should not be surprising since Figures 3 and 4 show that the largest variation in skin reflectance with oxygen saturation (S_{O2}) occurs around 560 nm and the isosbestic wavelength that is farthest from 560 nm is 500 nm. We should therefore expect that a reference (isosbestic) channel centered at 500 nm and a test channel (non-isosbestic) with peak sensitivity at 560 nm would be good candidate wavelengths for a two-channel imaging oximeter.
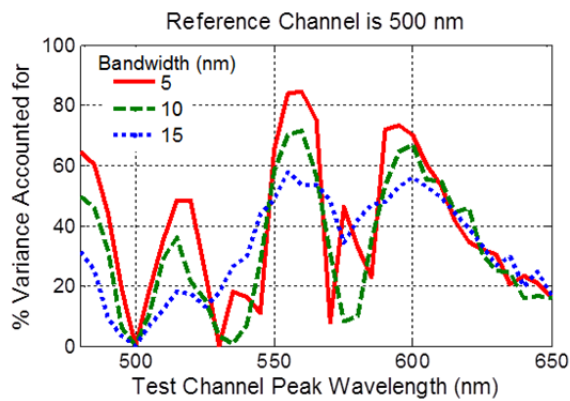

Figure 5: Correlation between the ratio of sensor responses and S_{O2}, expressed as the percentage of the variance in S_{O2} ($r^2 * 100$), plotted as a function of the peak wavelength sensitivity of the test channel, with bandwidth as the parameter.
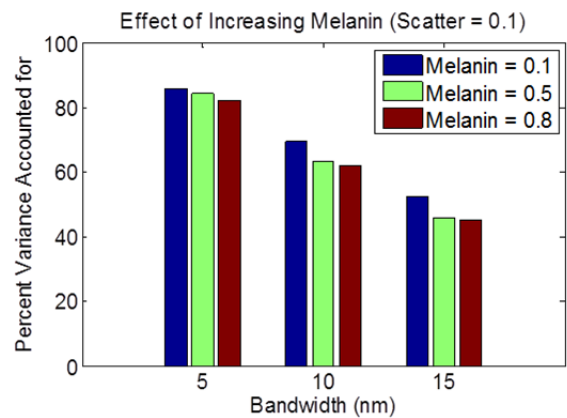
Figure 6: Effect of increasing melanin concentration on correlation between the ratio of sensor responses and S_{O2} , expressed as the percentage of the variance in S_{O2} ($r^2 * 100$).

Figure 5 also shows that the correlation between the ratio of sensor responses and S_{O2} decreases with increasing bandwidth. This result is also to be expected since the wider the bandwidth the more likely the reference channel and the test channel will integrate parts of the reflectance signal that increase with S_{O2}, with parts of the signal that decrease with S_{O2}.

Figure 6 shows that the correlation between the ratio of sensor responses and S_{O2} decreases with increasing concentrations of melanin. This result is consistent with the observation that it is difficult to estimate $S_{O2 in}$ skin that has high concentrations of melanin.

5. DISCUSSION AND SUMMARY

The purpose of this paper is to illustrate how computer simulations can be used to guide the design of imaging sensors for biomedical applications, such as measuring the percentage of oxygenated blood. The simulations make it possible to vary the illuminant, optics, and sensor in order to obtain the configuration most optimized for measuring oxygen saturation.

We used a weighted combination of absorbance functions for oxy-hemoglobin, deoxy-hemoglobin, melanin, and light scatter to generate skin reflectances. We show that the linear model for skin components can predict measurements of skin reflectances between 480 and 700 nm After validating the model over this range of wavelengths, we used the model to simulate skin reflectances with varying amounts of oxygen saturation.

Skin reflectances generated with different levels of S_{O2} were used as input to an ISET simulation of a two-channel imaging oximeter. The ISET simulations allowed us to evaluate the effectiveness of different combinations of two channels with different spectral sensitivities in predicting the S_{O2} levels. We found that the best predictions were obtained when the spectral sensitivities of the two channels were narrowband (~5 nm) with peak sensitivities centered at 500 and 560 nm, respectively. Increasing melanin concentration reduced the ability of the imaging oximeters to predict S_{O2} levels.

Our analysis is limited by the restricted range of wavelengths (480 – 700 nm) over which a simple linear model of skin absorbances can predict skin reflectances. At longer wavelengths, we know that the signal reaching the photodetector array is much smaller due to the fact that light is absorbed by water and lipids in the longer wavelengths. Furthermore, silicon photodetector arrays are much less sensitive to light in wavelengths greater than 700 nm. On the other hand, light in longer wavelengths can penetrate tissue to greater depths where arteries lie. And, as we noted earlier, most pulse oximeters use an LED with peak sensitivity at 940 nm and a half-amplitude bandwidth of 50 nm as the isosbestic channel and an LED with peak sensitivity at 660 nm and a half-amplitude bandwidth of 20 nm as the non-isosbestic channel. In the future, we plan to use empirical measurements of oxygen-deprived tissue to evaluate the design tradeoffs of imaging oximeters that use spectral channels that have peak sensitivities in the longer wavelengths and wider bandwidth.

Another future direction for this research is to determine whether existing imaging devices, such as RGB digital cameras and multispectral imaging systems, can be used to predict S_{O2} levels. We will also consider whether it is possible to use transverse field detectors [15, 16] to tune the spectral sensitivity of two or more channels in order to predict S_{O2} levels. To answer these questions, we are simulating imaging devices with more than two spectral channels and using linear combinations of the channel responses to predict S_{O2} levels. The methodology we describe in this paper serves as an important foundation for this ongoing research.

6. REFERENCES

[1]   R. D. Fiete, *Tutorial Texts in Optical Engineering* vol. TT92: SPIE Press, 2010.
[2]   J. Farrell, *et al.*, "A simulation tool for evaluating digital camera image quality," *Proceedings of the SPIE,* vol. 5294, pp. 124-131, 2004.
[3]   J. E. Farrell, *et al.*, "Digital camera simulation," *Applied Optics,* vol. 15, pp. 84-90, 2012.
[4]   J. Farrell, *et al.*, "Sensor calibration and simulation," *Proceedings of the SPIE,* vol. 6817, 2008.
[5]   J. Farrell, *et al.*, "Using visible SNR (vSNR) to compare the image quality of pixel binning and digital resizing," *Proceedings of SPIE,* vol. 7537, 2010.
[6]   J. Farrell, *et al.*, "Resolution and light sensitivity tradeoff with pixel size," *Proceedings of the SPIE* vol. 6069, 2006.
[7]   J. Chen, *et al.*, "Digital Camera Imaging System Simulation," *IEEE Transactions On Electron Devices* vol. 56, pp. 2496-2505, 2009.
[8]   Z. Smith, *et al.*, "Cell-Phone-Based Platform for Biomedical Device Development and Education Applications," *PLoS One,* vol. 6, 2011.
[9]   S. Seo, *et al.*, "Lensfree holographic imaging for on-chip cytometry and diagnostics," *Lab Chip,* vol. 9, pp. 777-787, 2009.
[10]   V. Pamplona, *et al.*, "NETRA: interactive display for estimating refractive errors and focal range," *ACM Trans. Graph.,* vol. 29, pp. 1-8, 2010.
[11]   L. L. Randeberg, *et al.*, "Hyperspectral imaging of bruised skin," *Proceedings of the SPIE,* vol. 6079, 2006.
[12]   G. Zonios, *et al.*, "Skin melanin, hemoglobin, and light scattering properties can be quantitatively assessed in vivo using diffuse reflectance spectroscopy," *The Journal of Investigative Dermotology,* vol. 117, pp. 1452 - 1457, 2001.

[13]   D. Yudovsky, *et al.*, "Hyperspectral imaging in diabetic foot wound care," *Journal of Diabetes Science and Technology,* vol. 4, pp. 1099 - 1113, 2010.

[14]   K. J. Zuzak, *et al.*, "Visible Reflectance Hyperspectral Imaging: Characterization of a Noninvasive, in Vivo System for Determining Tissue Perfusion," *Analytical Chemistry* vol. 74, pp. 2021-2028, 2002.

[15]   G. Langfelder, "Spectrally reconfigurable pixels for dual-color-mode imaging sensors," *Appl. Opt.,* vol. 51, pp. A91-A98, 2012.

[16]   G. Langfelder, *et al.*, "Tunable Spectral Responses in a Color-Sensitive CMOS Pixel for Imaging Applications," *Electron Devices, IEEE Transactions on,* vol. 56, pp. 2563-2569, 2009.

[17]   P. B. Catrysse and B. A. Wandell, "Integrated color pixels in 0.18-um complementary metal oxide semiconductor technology," *J. Opt. Soc. Am. A,* vol. 20, pp. 2293-2306, 2003.

[18]   G. Langfelder, *et al.*, "Tunable Spectral Responses in a Color-Sensitive CMOS Pixel for Imaging Applications," *IEEE Transactions On Electron Devices,* vol. 56, pp. 2563-2569, 2009.

[19]   F. Zaraga and G. Langfelder, "White balance by tunable spectral responsivities" *Journal of the Optical Society of America A.,* vol. 27, pp. 31-39, 2010.

[20]   J. G. Webster, ed. *Design of Pulse Oximeters*: Institute of Physics Publishing,, 1997.

[21]   R. R. Anderson and J. A. Parrish, "The Optics of Human Skin," *The Journal of Investigative Dermotology,* vol. 77, pp. 13-19, 1981.

[22]   M. J. C. V. Gemert, *et al.*, "Skin Optics," *IEEE Transcations on Biomedical Engineering,* vol. 36, pp. 1146-1154, 1989.

[23]   I. Nishidate, *et al.*, "Noninvasive imaging of human skin hemodynamics using a digital red-green-blue camera," *Journal of Biomedical Optics,* vol. 16, 2011.

[24]   A. Vogel, *et al.*, "Using noninvasive multispectral imaging to quantitatively assess tissue vasculature," *Journal of Biomedical Optics,* vol. 12, 2007.

[25]   D. Yudovsky and L. Pilon, "Retrieving skin properties from in vivo spectral reflectance measurements," *Journal of Biophotonics,* vol. 4, pp. 305–314, 2011.

[26]   M. Parmar, S. Lansel, J. Farrell, "An LED based lighting systems for acquiring multispectral scenes", *Proceedings of the SPIE*, vol. 8299, 2012

[27]   K. Martinez, *et al.*, "Ten Years of Art Imaging Research," *Proceedings of the IEEE,* vol. 90, pp. 28-41, 2002.

[28]   P. E. Bickler, *et al.*, "Effect of skin pigmentation on pulse oximeter accuracy at low saturation," *Anesthesiology,* vol. 102, pp. 715-719, 2005.

[29]   J. R. Feiner, *et al.*, "Dark skin decreases the accuracy of pulse oximeters at low oxygen saturation: the effects of oximeter probe type and gender," *Anesthesia & Analgesia,* vol. 105, 2007.